

Near-infrared quantum cutting via resonant energy transfer from Pr^{3+} to Yb^{3+} in LaF_3

K. Deng · X. Wei · X. Wang · Y. Chen · M. Yin

Received: 15 April 2010 / Published online: 10 February 2011
© Springer-Verlag 2011

Abstract Experimental evidence of energy transfer from Pr^{3+} to Yb^{3+} were presented by the excitation spectra and emission spectra in $\text{LaF}_3:\text{Pr}^{3+}, \text{Yb}^{3+}$. Temperature-dependent infrared emission and fluorescence decay curves have been measured to investigate the quantum cutting mechanism and energy transfer efficiency of the $\text{Pr}^{3+}-\text{Yb}^{3+}$ couple. Upon excitation of Pr^{3+} at 442 nm, Yb^{3+} emits two near-infrared photons around 1000 nm through two resonant energy transfer processes from Pr^{3+} to Yb^{3+} and the maximum total quantum efficiency reaches 161.6%. The excellent luminescence properties of the $\text{Pr}^{3+}-\text{Yb}^{3+}$ codoped LaF_3 indicate its potential application in improving the energy conversion efficiency of the silicon based solar cells by converting one blue photon to two near-infrared ones.

1 Introduction

Since the first report of an excellent quantum efficiency close to 200% in vacuum ultraviolet excited $\text{LiGdF}_4:\text{Eu}$ [1], there have been increasing research efforts in the quantum cutting materials; especially much interest has been paid to the development of highly efficient vacuum ultraviolet excited phosphors for applications such as plasma displays and mercury-free fluorescent lamps. The possibility of the large down-conversion efficiency is based on the principle that quantum cutting phosphors could generate two low-energy photons for every incident high energy photon absorption. Now, the investigation on quantum cutting phosphors has

been extended to the near-infrared region due to their potential application in improving the energy conversion efficiency of silicon-based solar cells. The process of cutting one ultraviolet or blue photon into two near-infrared lower-energy photons, which can both be better absorbed by the solar cells, can reduce the energy loss related to the thermalization of hot charge carriers, and thus may enhance the energy efficiency beyond the Shockley–Queisser limit.

The main systems of near-infrared quantum cutting phosphors include $\text{Tb}^{3+}-\text{Yb}^{3+}$ [2] and $\text{Tm}^{3+}-\text{Yb}^{3+}$ couple [3], in which Tb^{3+} and Tm^{3+} serves as the sensitizer and Yb^{3+} , the activator, emits photons at about 1000 nm, which can be efficiently absorbed by crystalline Si. However, the above mentioned couples exhibit a low energy transfer efficiency due to the second-order nature of cooperative energy transfer process. Therefore, it is important to develop a couple of sensitizer and activator in which a higher energy transfer efficiency can be achieved. The trivalent praseodymium Pr^{3+} is a promising candidate sensitizer for the near-infrared quantum cutting material since its absorption band is in the range of 420–490 nm, where the solar cells show poor spectrum response. However, the quantum cutting mechanism of the $\text{Pr}^{3+}-\text{Yb}^{3+}$ system is still controversial. In this paper, LaF_3 was chosen as a host to incorporate Pr^{3+} and Yb^{3+} to investigate the energy transfer efficiency and quantum cutting mechanism. Its relatively low phonon energy leads to low non-radiative transition rates due to multiphonon relaxation and high radiative transition rates, which increase the quantum efficiency.

2 Experimental section

Crystalline powder samples of LaF_3 doped with Pr^{3+} (0.5 mol%) and Yb^{3+} (0, 1, 3, 5, 10 mol%) were prepared

K. Deng · X. Wei · X. Wang · Y. Chen (✉) · M. Yin
Department of Physics, University of Science and Technology
of China, Hefei, 230026, China
e-mail: yuchen@ustc.edu.cn
Fax: +86-551-3607417

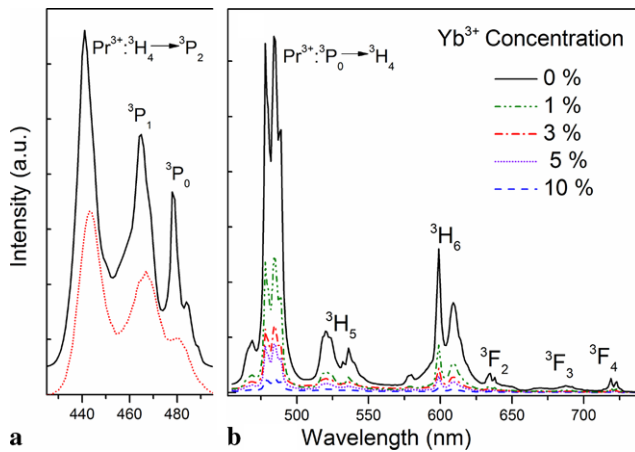


Fig. 1 (a) Excitation spectra of $\text{Pr}^{3+}:^3\text{P}_0 \rightarrow ^3\text{H}_6$ emission at 600 nm (solid curve) and $\text{Yb}^{3+}:^2\text{F}_{5/2} \rightarrow ^2\text{F}_{7/2}$ emission at 998 nm (dot curve) in 0.5% Pr^{3+} /3% Yb^{3+} codoped sample. (b) Visible emission spectra of the samples with different Yb^{3+} concentration under 442 nm excitation at 300 K

by coprecipitation method, using $\text{La}(\text{NO}_3)_3$, $\text{Pr}(\text{NO}_3)_3$, $\text{Yb}(\text{NO}_3)_3$, and NH_4HF_2 as raw materials. The remaining excess of NO_3^- and F^- in the obtained precipitations was removed by washing several times with distilled water. The products were dried at 50°C for 12 h and then calcined at 500°C for 2 h in a reduced atmosphere. All the samples were synthesized under identical conditions. The crystal structure was characterized by X-ray diffraction. Emission spectra, excitation spectra, and decay curves were detected by fluorescence spectrometer (Jobin-Yvon Fluorolog 3 system equipped with 450 W xenon lamp as the excitation source and with a Hamamatsu R928 photomultiplier as well as a liquid nitrogen-cooled DSS-IGA020L InGaAs detector).

3 Results and discussion

From the X-ray diffraction pattern of $\text{Yb}_x\text{La}_{0.995-x}\text{F}_3:\text{Pr}_{0.005}$ ($x = 0, 1, 3, 5, 10\%$), the samples are all hexagonal single phase. Luminescence properties are recorded to give convincing evidences for the existence of energy transfer from Pr^{3+} to Yb^{3+} . In Fig. 1(a) the excitation spectra of the $\text{Yb}^{3+}:^2\text{F}_{5/2} \rightarrow ^2\text{F}_{7/2}$ emission at 980 nm is very similar to the excitation spectra of the $\text{Pr}^{3+}:^3\text{P}_0 \rightarrow ^3\text{H}_6$ emission at 600 nm. The slight difference of the peak position arises from the experimental error of the detection system since the visible detector and the infrared detector are different. For the spectra monitoring the $\text{Pr}^{3+}:^3\text{P}_0 \rightarrow ^3\text{H}_6$ emission, the excitation peaks around 442, 467, 481 nm are assigned to the well-known $^3\text{H}_4 \rightarrow ^3\text{P}_{2,1,0}$ transitions, respectively. The observation of the $\text{Pr}^{3+}:^3\text{H}_4 \rightarrow ^3\text{P}_{2,1,0}$ lines in the excitation spectrum of Yb^{3+} shows the presence of energy transfer from Pr^{3+} to Yb^{3+} .

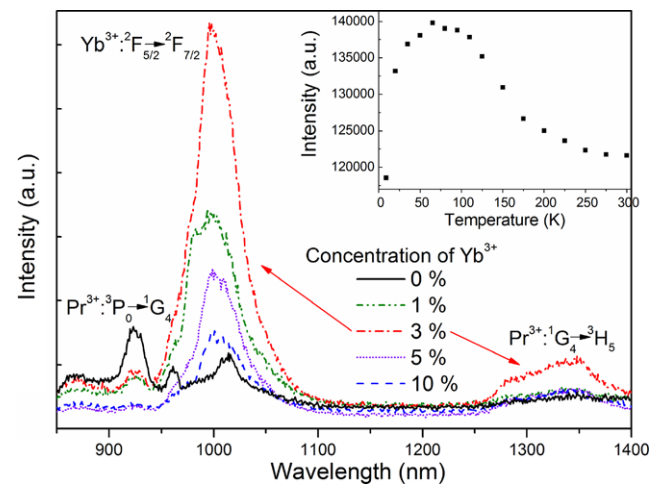


Fig. 2 Infrared emission spectra of the samples with different Yb^{3+} concentration under 442 nm excitation at 300 K. *Inset* shows the infrared emission (998 nm) intensity of Yb^{3+} under 442 nm excitation for various temperature in 0.5% Pr^{3+} /3% Yb^{3+} codoped sample

As is expected, due to the relatively large energy gap between the $^3\text{P}_0$ and $^1\text{D}_2$ level and the low phonon energy involved in LaF_3 , the Pr^{3+} single-doped sample shows the characteristic $^3\text{P}_0$ emission of Pr^{3+} upon 442 nm excitation in Fig. 1(b) and is in agreement with the previous literature [4]. Besides, in the $\text{Pr}^{3+}-\text{Yb}^{3+}$ codoped samples a broad emission band around 1000 nm under the same excitation wavelength has also been observed in Fig. 2 and it corresponds to the $^2\text{F}_{5/2} \rightarrow ^2\text{F}_{7/2}$ transition of Yb^{3+} . With the increase of Yb^{3+} concentration the visible emission from Pr^{3+} weakens monotonically, while the near-infrared emission of Yb^{3+} intensifies. However, an obvious decrease of the Yb^{3+} emission intensity has been observed when the Yb^{3+} concentration reached 5%, owing to the concentration quenching effect. Upon excitation at 442 nm, apart from the infrared emission from Yb^{3+} , infrared emission around 923 nm and 1350 nm, originating from the $\text{Pr}^{3+}:^3\text{P}_0 \rightarrow ^1\text{G}_4$ and $^1\text{G}_4 \rightarrow ^3\text{H}_5$, respectively, are also detected in the $\text{Pr}^{3+}-\text{Yb}^{3+}$ codoped samples. However, in the previous reports [5, 6], such emission had not been noticed.

Luminescence decay curves recorded for emission from the $^3\text{P}_0$ level provide further insight into the transfer efficiency. In Fig. 3, the decay curves of the $\text{Pr}^{3+}:^3\text{P}_0 \rightarrow ^3\text{H}_4$ emission at 484 nm with logarithmic coordinates are plotted with various Yb^{3+} concentration to investigate the lifetime of the $^3\text{P}_0$ level. The $\text{Pr}^{3+}:^3\text{P}_0 \rightarrow ^3\text{H}_4$ emission in Pr^{3+} single doped sample shows a nearly single exponential decay as expect. As can be seen from the inset in Fig. 3, when the Yb^{3+} concentration is increased from 0 to 10%, the decay time declines from 111.3 to 40.8 μs . The faster decay as a function of Yb^{3+} concentration can be explained by the introduction of extra decay pathways due to the Yb^{3+} doping: energy transfer from $\text{Pr}^{3+}:^3\text{P}_0$ to Yb^{3+} enhances the Pr^{3+}

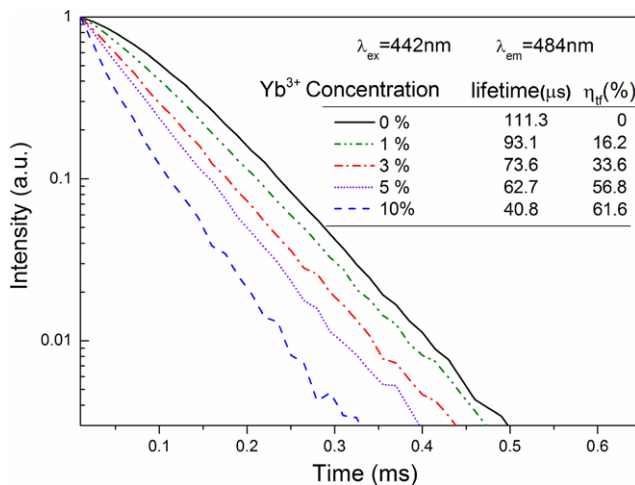


Fig. 3 Decay curves of the Pr^{3+} $^3\text{P}_0 \rightarrow ^3\text{H}_4$ emission at 484 nm under 442 nm excitation. Inset shows the decay lifetime, energy transfer efficiencies η_{tf} , and quantum efficiencies η_q versus Yb^{3+} concentration

$^3\text{P}_0$ decay rate. From the luminescence decay curves an estimate of overall energy transfer efficiency ($\eta_{\text{tr},x\%Yb}$) and quantum efficiency ($\eta_{x\%Yb}$) can be obtained using the following equations [7]:

$$\eta_{\text{tr},x\%Yb} = 1 - \frac{\int I_x\%Yb dt}{\int I_{10\%Yb} dt}, \quad (1)$$

$$\eta_{x\%Yb} = \eta_{\text{Pr}}(1 - \eta_{\text{tr},x\%Yb}) + 2\eta_{\text{Yb}}\eta_{\text{tr},x\%Yb}, \quad (2)$$

where I denotes the decay intensity and $x\%$ stands for the Yb^{3+} concentration. η_{Pr} and η_{Yb} represent the quantum efficiency of Pr^{3+} and Yb^{3+} , and both of them are set to 1. The values of energy transfer efficiencies and quantum efficiencies versus Yb^{3+} concentration are summarized in the inset of Fig. 3. With the increase of Yb^{3+} concentration from 1 to 10%, the energy transfer efficiency increases monotonically from 16.2% to 61.6%. For the 0.5% Pr^{3+} and 10% Yb^{3+} doped sample, quantum efficiency reaches a maximum of 61.6% by ignoring the nonradiative losses. However, the existence of concentration quenching even at an Yb^{3+} concentration of 5% poses an obstacle to much higher quantum efficiency.

Compared with the Tb^{3+} - Yb^{3+} and Tm^{3+} - Yb^{3+} codoped systems [2, 3], the energy transfer from Pr^{3+} to Yb^{3+} is efficient at relatively low Yb^{3+} concentration. A simple estimate of the energy transfer rate P_{tf} can be obtained with the following equation:

$$\frac{1}{\tau_{\text{Pr}}} + P_{\text{tr}} = \frac{1}{\tau_{\text{Pr}-\text{Yb}}} \quad (3)$$

$\tau_{\text{Pr}-\text{Yb}}$ and τ_{Pr} denotes the measured lifetime of Pr^{3+} $^3\text{P}_0$ level in the presence and absence of Yb^{3+} doping, respectively. For the sample with 0.5% Pr^{3+} and 3% Yb^{3+} doping, according to the formulas mentioned above, it results in an

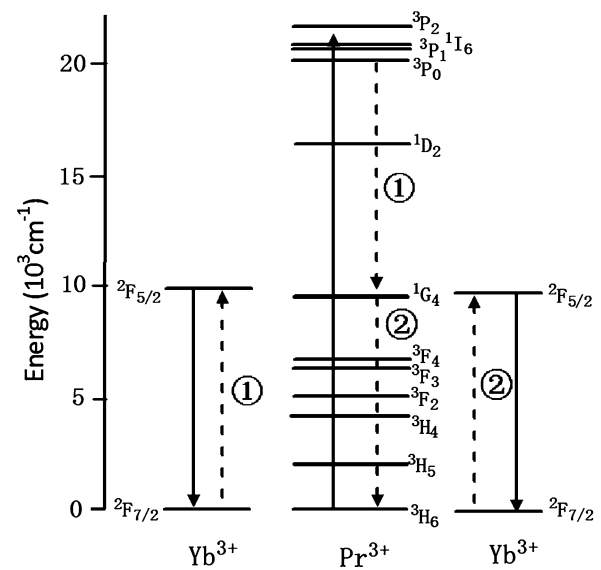


Fig. 4 Energy level diagrams showing the quantum cutting process involved a two-step energy transfer: cross-relaxation (indicated by ①) followed by another resonant energy transfer (indicated by ②)

energy transfer rate of $1.6 \times 10^4 \text{ s}^{-1}$, which is much faster than the radiative decay rate of Pr^{3+} (about $9.0 \times 10^3 \text{ s}^{-1}$), and thus indicates the efficient energy transfer process.

Further information about the quantum cutting mechanism can be obtained in the infrared emission spectra in Fig. 2. The infrared emission intensity of $^3\text{P}_0$ decreases with increasing Yb^{3+} concentration, while the $^1\text{G}_4$ emission intensifies until the concentration is greater than 3%. It can be ascribed to the cross relaxation between Pr^{3+} ($^3\text{P}_0 \rightarrow ^1\text{G}_4$) and Yb^{3+} ($^2\text{F}_{7/2} \rightarrow ^2\text{F}_{5/2}$) which depopulates the Pr^{3+} $^3\text{P}_0$ state but simultaneously populates the $^1\text{G}_4$ state of Pr^{3+} . When the Yb^{3+} concentration exceeds 3%, the infrared emission intensities of $^3\text{P}_0$ and $^1\text{G}_4$ under 442 nm excitation both decrease, which are consistent with the occurrence of energy transfer from the Pr^{3+} $^3\text{P}_0$ and $^1\text{G}_4$ states to Yb^{3+} . Besides, the Yb^{3+} infrared emission (998 nm) intensity is, however, temperature-dependent as can be seen in the inset of Fig. 2, due to the fact that the $^1\text{G}_4$ level of Pr^{3+} is at slightly lower energy (about 200 cm^{-1}) than the $^2\text{F}_{5/2}$ level of Yb^{3+} . As temperature is raised, phonons are available and phonon-assisted energy transfer rate grows so that the level mismatch does not hamper the energy transfer, coincident with the increase of Yb^{3+} near-infrared emission intensity. At higher temperature, the Yb^{3+} emission intensity decreases due to the energy transfer from Yb^{3+} to Pr^{3+} . However, in a cooperative energy transfer process the Yb^{3+} near-infrared emission intensity almost remains constant with increasing temperature [8]. Hereby in the Pr^{3+} - Yb^{3+} codoped system, we consider the energy transfer process to be first-order rather than cooperative energy transfer as explained in a similar process [5, 9].

An energy level diagram showing the process of quantum cutting is presented in Fig. 4. Upon excitation of the Pr^{3+} into the ${}^3\text{P}_{0,1,2}$ level, depopulation of the ${}^3\text{P}_0$ excited state can occur through two sequential steps with the ${}^1\text{G}_4$ level acting as an intermediate level: cross relaxation process mentioned above followed by resonant energy transfer from $\text{Pr}^{3+}({}^1\text{G}_4)$ to $\text{Yb}^{3+}({}^2\text{F}_{5/2})$. Consequently, the two-step transfer results in two Yb^{3+} ions in excited states, and thereby converting a blue photon absorbed by Pr^{3+} into two near-infrared photons originating from ${}^2\text{F}_{5/2}\rightarrow{}^2\text{F}_{7/2}$ transitions of Yb^{3+} . However, without an intermediate energy level, energy transfer from the ${}^5\text{D}_4$ level of Tb^{3+} to Yb^{3+} and the ${}^1\text{G}_4$ level of Tm^{3+} to Yb^{3+} could only proceed through a second-order cooperative energy transfer process. The much higher (typically a factor of 10^3) probability of the first-order energy transfer processes than the second-order processes also accounts for the reason why the Pr^{3+} – Yb^{3+} couple exhibits a high transfer efficiency for Yb^{3+} concentration as low as 10%.

4 Conclusion

In summary, Pr^{3+} – Yb^{3+} codoped LaF_3 crystalline powder samples have been investigated as a promising material to enhance the energy conversion efficiency of silicon based solar cells. Excitation, emission spectra, and decay curves indicate the occurrence of energy transfer from Pr^{3+}

to Yb^{3+} . We conclude that the energy transfer process from Pr^{3+} to Yb^{3+} involves two sequential resonant energy transfer rather than cooperative energy transfer. The quantum efficiency reaches 161.6% for Yb^{3+} concentration as low as 10%.

Acknowledgements This work was supported by National Nature Science Foundation of China (10774140, 11011120083 and 10904139), Knowledge Innovation Project of the Chinese Academy of Sciences (KJCX2-YW-M11), and Special Foundation for Talents of Anhui Province, China (2007Z021).

References

1. R.T. Wegh, H. Donker, K.D. Oskam, A. Meijerink, *Science* **283**, 663 (1999)
2. S. Ye, B. Zhu, J.X. Chen, J. Luo, J.R. Qiu, *Appl. Phys. Lett.* **92**, 141112 (2008)
3. L.C. Xie, Y.H. Wang, H.J. Zhang, *Appl. Phys. Lett.* **94**, 061905 (2009)
4. E.Y. Wong, O.M. Stafsudd, D.R. Johnston, *J. Chem. Phys.* **39**, 3 (1963)
5. D.Q. Chen, Y.S. Wang, Y.L. Yu, P. Huang, F.Y. Weng, *Opt. Lett.* **33**, 16 (2008)
6. X.P. Chen, X.Y. Huang, Q.Y. Zhang, *J. Appl. Phys.* **106**, 063518 (2009)
7. P. Vergeer, T.J.H. Vlugt, M.H.F. Kox, M.I. Den Hertog, J.P.J.M. van der Eerden, A. Meijerink, *Phys. Rev. B* **71**, 014119 (2005)
8. J.J. Zhou, Y.X. Zhuang, S. Ye, Y. Teng, G. Lin, B. Zhu, J.H. Xie, J.R. Qiu, *Appl. Phys. Lett.* **95**, 141101 (2009)
9. Q.Y. Zhang, G.F. Yang, Z.H. Jiang, *Appl. Phys. Lett.* **91**, 051903 (2007)